# Photoluminescence and electronic transition behaviors of single-stranded DNA

# Photoluminescence from single-stranded DNA structures

Qiujin Wang[1,#], Shuo Lin[1], Wen Xu[1,2,†], Changneng Liang[1], Lan Ding[1,*] & Francois M. Peeters[3]

[1]*School of physics and Astronomy and Key Lab of Quantum Information of Yunnan Province, Yunnan University, Kunming 650091, China.*

[2]*Key Laboratory of Materials Physics, Institute of Solid State Physics, Chinese Academy of Sciences, Hefei 230031, China.*

[3] *Department of Physics, University of Antwerp, Groenenborgerlaan 171, B-2020 Antwerpen, Belgium*

[*]*Corresponding author: dinglan@ynu.edu.cn*

†*Corresponding author: wenxu_issp@aliyun.com*

## Abstract

We present a systematic investigation of the photoluminescence (PL) from single-strand DNA (ssDNA) with different bases (T, A, C and G) and different base numbers (20, 35 and 56). We find that the features of the PL emission from these samples depend sensitively and characteristically on the base structure and base number of the ssDNA. The results obtained from the PL and PL excitation (PLE) measurements indicate that the dependence of the PL and PLE peak wavelengths upon the excitation wavelength can exhibit different features for ssDNA with different base structures and base numbers. Through examining the dependence of the PL and PLE peaks along with the amplitude of the PL peaks upon the excitation wavelength, we are able to identify optically the ssDNA with different bases and the same base but with different base numbers. Thus, one can achieve a non-invasive and label free characterization of the ssDNA by the

standard PL measurement. We also propose and examine the possible mechanisms for PL from ssDNA in different excitation wavelength regimes. It is found that the PL from ssDNA is akin to that from a direct band-gap semiconductor with radiative impurity states. This work is relevant to the application of the state-of-the-art optical technique for the characterization and investigation of the DNA structures.

**Introduction**

Deoxyribonucleic acid (DNA) is an essential carrier for the storage and transmission of genetic information in living organisms and many viruses. It is well known that the DNA molecules are usually comprised of two polynucleotide strands coiled around each other to form a double helix[1], in which the nucleotide, the monomer unit of each strand, contains nucleobases, deoxyribose and phosphoric acid. There are four kinds of nitrogen-containing nucleobases such as adenine (A), guanine (G), cytosine (C), and thymine (T). The DNA structure has been a center of attention for scientific research. Particularly, to flexibly form different nanostructures on the basis of the DNA, in 1982 Seeman and co-workers developed the technique of the sticky end joining for genetic engineering of single-strand DNA (ssDNA) [2]. Since then, the investigation of the DNA and ssDNA structures[3] along with the DNA nanotechnology[4-6] have become the hot and fast-growing field of research in life science, medicine, bio-nanotechnology, bio-chemistry and bio-physics.

Because the DNA molecules are basically with a double helix structure, various experimental approaches for physical studies have been utilized for relevant studies. In

particular, since 2000 the state-of-the-art optical techniques (e.g., resonant light-scattering, solid-substrate phosphorescence, fluorescent probe, fluorescent spectroscopy, etc.) have been applied for the investigation of the DNA. It was found via resonant light-scattering experiments that the organic dyes gathered around the nucleic acid can lead to the enhancement of the light scattering. This effect can be used for quantitative measurement of the nucleic acid[7,8]. By using solid-substrate phosphorescence method, the detection for much lower absolute limits can be achieved when the nucleic acid solution is spotted onto a solid substrate[9]. At present, fluorescent probe has been a popularly used optical approach for sensitive and selective detection of nucleic acids[10]. Moreover, fluorescent spectrometry has been widely applied for examining the energy band structure of the DNA[9-12]. It has also been found that the ligands and the fluorescent dyes can work nicely with ssDNA or DNA to enhance the signals of optical response. For example, in 2013 the physical coupling between the DNA tetrahedron and the Adriamycin has been realized experimentally. A strand of the DNA tetrahedron was labeled with fluorescent dye, showing significant cytotoxicity to multi-drug resistant cells[11], as well as imaging sentinel lymph nodes of fluorescently labeled DNA tetrahedron[12]. In recent years, the novel two-dimensional electronic materials (2DEMs, e.g., graphene oxide, monolayer $MoS_2$, etc.) have been employed for sensitive and selective detection of dye-labeled DNA and proteins[12-14]. Furthermore, it has been demonstrated that the DNA sequences can be combined with metal-based nanoparticles and nanostructures and, as a result, different bases of the DNA sequences can be clearly distinguished by, e.g., the fluorescent frequencies and intensities[13-18].

Because optical experiments are normally contactless, non-destructive and non-contaminative, coupled with their sensitivity and selectivity in the measurement, they have been a powerful and popularly used physics tool in the field of the DNA research.

It should be noted that in optical measurements of the DNA, as mentioned above, although the presence of the fluorescent agents (e.g., the dyes), modulators (e.g., the nano-particles and 2DEMs) and the probes can enhance the fluorescent signals from the DNA, these additional materials and probes usually can lead to complex measurement, high cost, and to the pollution of the DNA samples. Therefore, it is desirable and of the great importance and significance that one can measure optically and directly the as-grown DNA samples to obtain enough information about the nucleic acid structures. This becomes the prime motivation of the present study. Meanwhile, we notice that at present, little is known about the underlying mechanism of the photoluminescence (PL) from the DNA. We intend contributing an exploration in this aspect on the basis of the results obtained from this study.

In this work, we measure the PL spectra of label-free and probe-free ssDNA samples at different excitation wavelengths by using a standard technique. The ssDNA samples with sequences containing nucleobases of only one type of A or C or T or G structure with different base numbers are prepared and measured respectively. We also conduct the measurements and analysis of the PL excitation (PLE) spectra for these samples in order to identify different ssDNA samples via examining the dependence of the intensity and wavelength of the corresponding emission peaks upon the excitation wavelength. All the measurements in this study are carried out at room-temperature.

From these results, we can achieve a non-invasive and label-free detection and identification of the nucleic acid structures and can gain an in-depth understanding of the underlying mechanism of the PL emission from ssDNA.

## Results and Discussion

In this study, the ssDNA samples are prepared by using the technique of the solid-phase phosphite-triester method with an automatic synthesizer[19,20]. The samples with sequences containing different nucleobases are fabricated, here each ssDNA sample contains 28/35/56 bases of only one type of A or C or T or G. More details of the sample preparation can be found in Methods.

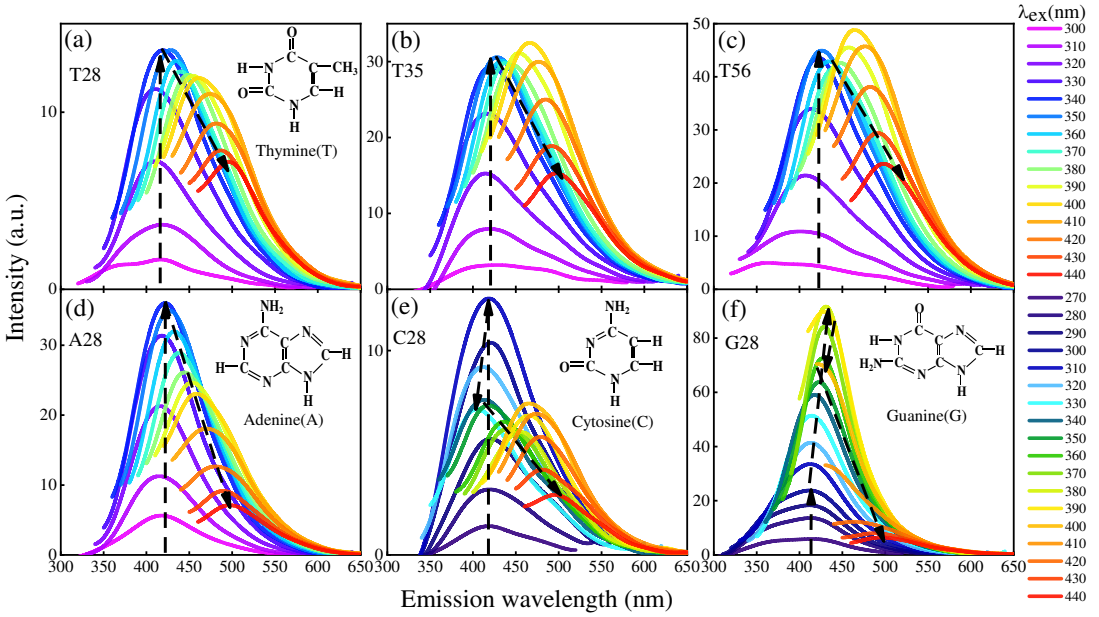


Fig.1 PL spectra for ssDNA samples with only T28, T35, T56, A28, C28 and G28 in respectively (a)-(f) at different excitation wavelengths as indicated. The dashed black lines indicate the movement trend of the peak positions and the insets show the corresponding nucleic acid structures.

In the present study, we first measure directly the PL spectra of the ssDNA samples and examine mainly the dependence of the PL peak wavelength ($\lambda_{em}$) upon the pumping or excitation wavelength ($\lambda_{ex}$). In Fig. 1, we show the PL spectra for ssDNA samples

with only T28, T35, T56, A28, C28, G28 base in (a)-(f) respectively at different excitation wavelengths. The dashed black lines are drawn to indicate the movement trend of the corresponding peak positions. For the case of base T [see Fig. 1(a)-(c)], we find that: i) in relatively short $\lambda_{ex}$ regime, the intensity of the PL emission from T-based ssDNA with different base numbers $N$ increases with $\lambda_{ex}$, while the peak position depends very little on $\lambda_{ex}$; ii) in sharp contrast, in relatively long $\lambda_{ex}$ regime, the PL intensity decreases and the red-shift of the peak position can be observed with increasing $\lambda_{ex}$; and iii) however, the spectral line shapes and the trend of their variations with $\lambda_{ex}$ are not sensitive to the base number $N$, while the PL intensity increases with increasing $N$. Accordingly, we can focus our attention on the effect of different bases but with the same $N$ number (i.e., A28, C28, T28, and G28 in Fig. 1). It can be seen clearly that the variation trend with $\lambda_{ex}$ for T28 is in line with that for A28, while that for C28 is similar to that for G28, as shown in Fig 1(a, d-f). These interesting findings suggest that the base type of the ssDNA can affect significantly the basic features of the PL spectra measured at different excitation wavelength regimes.

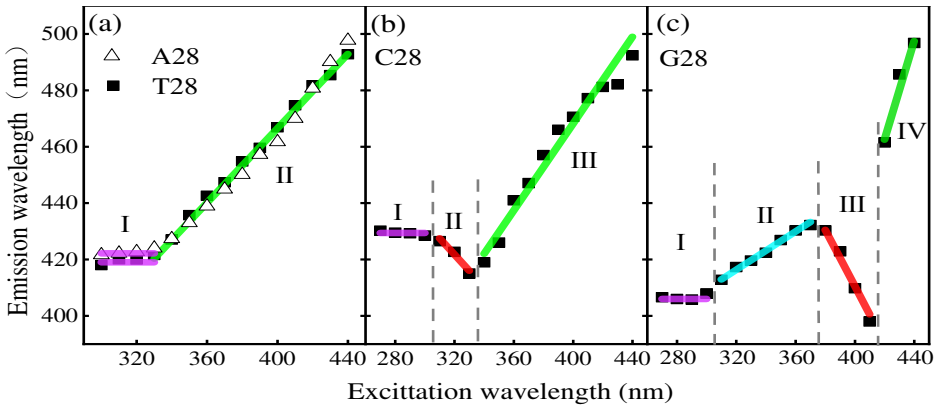


Fig.2 Peak wavelength of the PL emission, $\lambda_{em}$, as a function of excitation wavelength, $\lambda_{ex}$, for A28 and T28 in (a), C28 in (b) and G28 in (c). Here, the square and triangular dots are experimental results, the corresponding lines are fitting results, and the vertical dashed lines are drawn in (b) and (c) to indicate different excitation wavelength regimes.

With the results shown in Fig. 1, we can plot the peak wavelength in PL spectrum ($\lambda_{em}$) as a function of the excitation wavelength ($\lambda_{ex}$) for ssDNA with different bases (T, A, C, G) at a fixed base number $N$=28, as shown in Fig. 2. Firstly, we note that in short excitation wavelength regime (I), $\lambda_{em}$ for T-, A-, C-, and G-based ssDNA depend very weakly on $\lambda_{ex}$, where $\lambda_{em}$=419 nm for T28, 422 nm for A28, 430 nm for C28, and 406 nm for G28 respectively. These results imply that in this $\lambda_{ex}$ regime, i) the PL emission from a ssDNA sample is mainly induced by exciton-like electronic transitions via combination and separation of the electron-hole pairs[21]; ii) the energy difference between the LUMO and HOMO states for excitonic transitions differs for ssDNA with different bases; and iii) the maximum excitation wavelength $\lambda_{exm}$ for this regime also differs for different ssDNA samples, where $\lambda_{exm}$=330 nm for T28 and A28 and 300 nm for C28 and G28 respectively. Secondly, at long wavelength excitations ($\lambda_{ex}$> $\lambda_{exm}$), $\lambda_{em}$ from ssDNA depends strongly on $\lambda_{ex}$ and different samples show different dependences. It is interesting to note that for T28 and A28 samples, $\lambda_{em}$ depends roughly linearly on $\lambda_{ex}$ so that we can fit $\lambda_{em}= a\lambda_{ex}+b$, where a=0.66 and b=202.5 nm for both of them. In contrast, the dependence of $\lambda_{em}$ upon $\lambda_{ex}$ for C28 and G28 samples differs in different $\lambda_{ex}$ regimes. For C28, the $\lambda_{em}$~$\lambda_{ex}$ relation can be divided into three different regions denoted by I, II and III respectively in Fig. 2(c), where $\lambda_{em}$=430 nm in region I ($\lambda_{ex}$<300 nm) and $\lambda_{em}=a\lambda_{ex}+b$ with $a=-0.58$ and $b=606.8$ nm in region II ($\lambda_{ex}$=300~340 nm) and $a=0.77$ and $b=160.2$ nm in region III ($\lambda_{ex}$>340 nm). The $\lambda_{ex}$~$\lambda_{em}$ relations in regions I and III are similar to the case of A28 and T28. However, in region II, the $\lambda_{ex}$~$\lambda_{em}$ relation is anomalous, where a linear like blue-shift of $\lambda_{em}$ with increasing $\lambda_{ex}$ can be observed.

For G28, the $\lambda_{em}$~$\lambda_{ex}$ relation can be divided into four different regions as shown in Fig. 2(d), where $\lambda_{em}$=406 nm in region I ($\lambda_{ex}$<300 nm) and in regions II ($\lambda_{ex}$=300~370 nm), III (380~410 nm) and IV ($\lambda_{ex}$>420 nm), we can fit $\lambda_{em}=a\lambda_{ex}+b$ with respectively $a=0.34$ and $b=307.5$ nm in II, $a=-1.0$ and $b=810.5$ nm in III and $a=1.75$ and $b=-272.5$ nm in IV. Similar to C28, the blue-shift of $\lambda_{em}$ with increasing $\lambda_{ex}$ can be observed in region III for G28. Thirdly, from the results shown in Fig. 2 and discussed above, we would like to point out that when $\lambda_{ex}$> $\lambda_{exm}$, i) a roughly the same $\lambda_{em}$~$\lambda_{ex}$ relation for T28 and A28 can be understood by the fact that the T- and A-base in ssDNA have the same complementary base pairing structure[1,22]; ii) according to the principle of the complementary pairing for C- and G-base[1,23], the main features of the PL from G28 (e.g., $\lambda_{em}$, $\lambda_{exm}$, linear dependence of $\lambda_{em}$ upon $\lambda_{ex}$, etc) should be analogical to the case of C28. However, due to different ring structures for C- and G-base, the difference of the $\lambda_{ex}$~$\lambda_{em}$ relations for C28 and G28 is mainly induced by the fact that the C-base is with a single ring structure (see inset in Fig. 1(e)), whereas the G-base has a double ring structure (see inset in Fig. 1(f)) which is associated with the strong dipole-dipole coupling between the ssDNA molecules and the double distilled water (dd-water)[24,25]; and iii) the main physical mechanism behind the blue-shift of $\lambda_{em}$ with increasing $\lambda_{ex}$, observed in region II for C28 and in region III for G28, is associated with the ground-state dimer formed by pyrene molecular solution[26]. One of the most important findings from Fig. 2 is that the peak wavelength of the PL spectrum depends differently on excitation wavelength for ssDNA with different bases.

From a viewpoint of physics, the dependence of $\lambda_{em}$ upon $\lambda_{ex}$ in an electronic

system should rely also on the electronic transition channels. As discussed above, when $\lambda_{ex} < \lambda_{exm}$, the PL from a ssDNA is mainly induced by exciton-like electronic transitions and the peak wavelength $\lambda_{em}$ corresponds to the energy difference between the LUMO and HOMO states in ssDNA. To look into the electronic transition channels for PL in the case of $\lambda_{ex} > \lambda_{exm}$, we undertake the PL excitation (PLE) measurement on ssDNA samples. Here the PLE spectrum is obtained by fixing an emission wavelength $\lambda_{em}$ and scanning the excitation wavelength $\lambda_{ex}$. Since the results for A- and T-base samples should be roughly similar (see Figs. 1 and 2), here we first take the T-base samples as the example for the investigation and analysis. The PLE spectra for T28, T35 and T56 are shown in Fig. 3(a) at a fixed $\lambda_{em}$=419 nm and in Fig. 3(b) at a fixed longer $\lambda_{em}$=450 nm. As we can see, the intensity of the PLE increases with the base number N, while only one PLE peak can be observed at about $\lambda_{ex}$=345 nm for $\lambda_{em}$=419 nm and two peaks can be measured for $\lambda_{em}$=450 nm. We find that the line shape of the PLE spectrum can be fitted nicely by a Gaussian-like profile. For the case of $\lambda_{em}$=450 nm, two PLE peaks at about $\lambda_{ex}$=345 nm and 397 nm can be obtained via Gaussian fitting (dotted curves), which implies that there are two transition channels for PL emission at a wavelength $\lambda_{em}$=450 nm. We know that the unchanged dimer luminescence channel is with a transition energy or wavelength $\lambda_{ex}$=345 nm (see Fig. 3(a)). The PLE peak at $\lambda_{ex}$ =397 nm is induced by water luminescence[27]. Therefore, for a T- or A-based ssDNA sample, the PLE spectrum measured at a relatively short emission wavelength is mainly induced by dimer luminescence and that measured at a relatively long emission wavelength can be attributed to the coupling between T- or A-base with water.

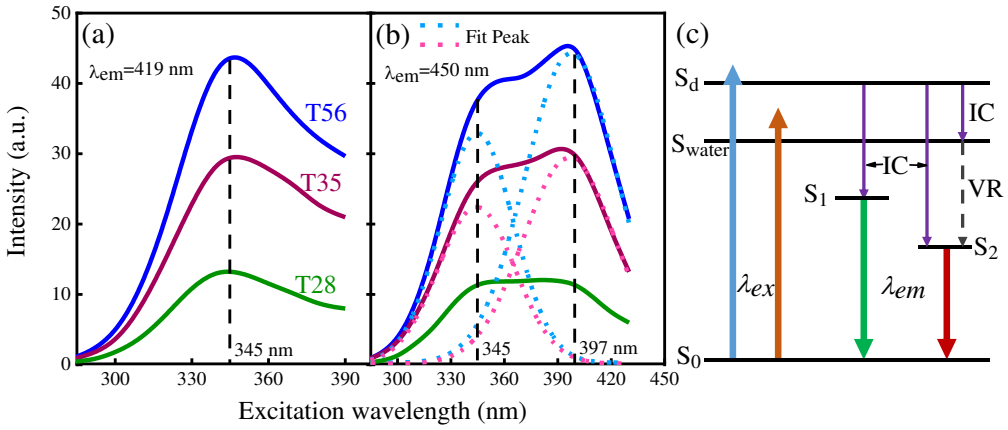


Fig. 3 PLE spectra measured at the fixed emission wavelength $\lambda_{em}$=419 nm in (a) and $\lambda_{em}$=450 nm in (b) for T28, T35 and T56 samples. The diagram of the energy levels and the corresponding electronic transitions is shown in (c), where $S_j$ refers to different energy levels and IC and VR are respectively for internal conversion and vibrational relaxation.

With the results shown in Fig. 3(a, b), we can build up the diagram for energy levels and the electronic transition accompanied by the corresponding photo-physics process in T- and A-based ssDNA, as shown in Fig. 3(c). In this diagram, the high energy levels which can absorb photo-excited electrons from occupied low energy states ($S_0$) are the dimer states ($S_d$) in ssDNA and water molecule states ($S_{water}$). They are very stable[28] for ssDNA in water. There are two kinds of radiative electronic states in low energy regime with the higher ($S_1$) and lower ($S_2$) levels. When excitation phonon energy is larger than $E(S_d)$-$E(S_0)$ (i.e., $\lambda_{ex}$<345 nm), the electrons in $S_0$ states can be pumped into the $S_d$ states. The photo-induced electrons in the $S_d$ levels can be relaxed quickly into the $S_1$ levels via non-radiative internal conversion (IC)[29,30], here we name it as process I (PI). Meanwhile, these electrons can also be relaxed into the $S_2$ levels via combined channels from $S_d$ levels to $S_2$ levels directly by the IC and from $S_d$ to $S_{water}$ by vibrational relaxation (VR)[30,31] and then from $S_{water}$ to $S_2$ by the IC again, here we name this process as II (PII). Because the PII requires a larger energy transfer

than the PI, PII is much slower than PI in terms of the electronic relaxation time. Therefore, for PLE measured at a shorter $\lambda_{em}$=419 nm, only one peak can be observed at $\lambda_{ex}$~345 nm, which corresponds to dimer luminescence transition. When excitation phonon energy is in-between $E(S_d)$-$E(S_0)$ and $E(S_{water})$-$E(S_0)$ (i.e., 345<$\lambda_{ex}$<397 nm), the electrons in $S_0$ states can only be pumped into the $S_{water}$ states. The photo-induced electrons in $S_{water}$ states can be relaxed into the $S_2$ states via non-radiative IR mechanism. As a result, for PLE measured at a longer $\lambda_{em}$=450 nm, two peaks can be observed at $\lambda_{ex}$~345 nm and $\lambda_{ex}$~397 nm, where the peak at $\lambda_{ex}$~397 nm can be attributed to the coupling between the T- or A-base with water.

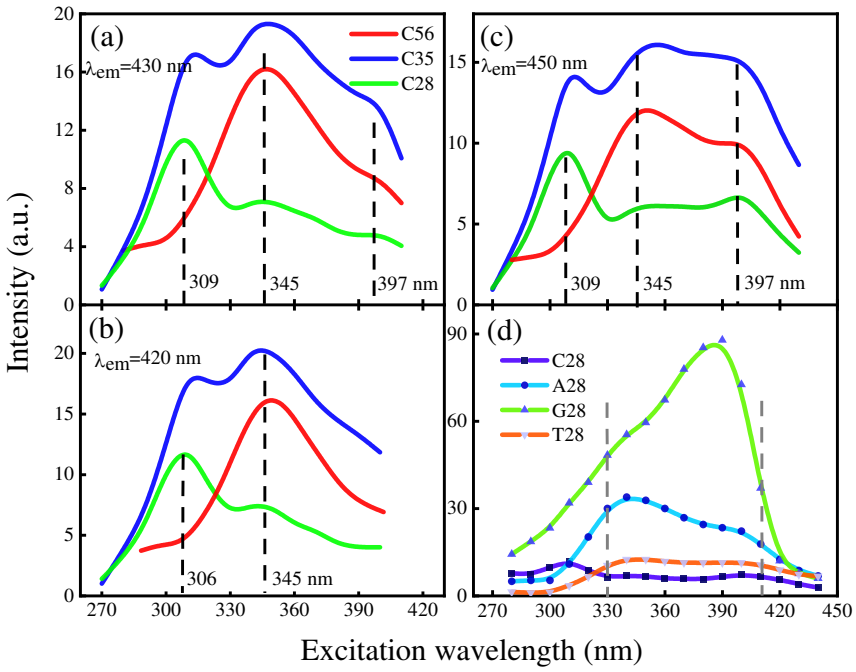


Fig. 4 PLE spectra measured at the fixed emission wavelength $\lambda_{em}$=430 nm in (a), $\lambda_{em}$=420 nm in (b) and $\lambda_{em}$=450 nm in (c) for C28, C35 and C56 samples, where the vertical dashed lines indicate the positions of the peaks. The amplitude of the PL peaks for T28, A28, C28 and G28 as a function of excitation wavelength is shown in (d).

In Fig. 4 we show the PLE spectra measured at the fixed emission wavelength $\lambda_{em}$=430 nm in (a), $\lambda_{em}$=420 nm in (b) and $\lambda_{em}$=450 nm in (c) for C28, C35 and C56

samples. From Fig. 2(b), we learn that $\lambda_{em}$=430 nm, 420 nm and 450 nm regard respectively to the excitation wavelength regions I, II and III. For C28 (green curves), there is a clear PLE peak (Peak 1) at 309 nm for $\lambda_{em}$=430 nm, at 306 nm for $\lambda_{em}$=420 nm and at 309 nm for $\lambda_{em}$=450 nm. This peak is caused mainly by the formation of the transition channel due to the coupling of the double hydrogen bonds between C-base and dd-water[23]. Two weak PLE peaks (Peak 2 and 3) can also be found respectively at 345 nm and 397 nm, which are independent on $\lambda_{em}$. As been discussed above, Peak 2 and 3 come from electronic transition channels for, respectively, the dimer and water luminescences. For C35 (blue curves), the Peak 1 is shifted to 313 nm for $\lambda_{em}$=420 nm and to 312.5 nm for $\lambda_{em}$=450 nm. This is because the interaction of the double hydrogen bonds between the C-base and dd-water depends on the base numbers. The Peak 2 can be seen for $\lambda_{em}$=420 nm where the Peak 3 cannot be measured. This is the case observed and discussed for T28 measured at a relatively short wavelength of $\lambda_{em}$ (see Fig. 3(a)). In contrast, both the Peak 2 and Peak 3 can been observed for $\lambda_{em}$=450 nm, corresponding the case observed and discussed for T28 measured at a relatively long wavelength of $\lambda_{em}$ (see Fig. 3(b)). For C56 (red curves), the Peak 1 cannot be observed. It is known that in a phosphinic acid with nitrogen-base structures, the symmetry of the hydrogen bonds and the corresponding polarizability can become significantly weaker with increasing basicity and/or nitrogen-base number[32]. Similar to this mechanism, the interaction of the double hydrogen bonds between the C-base in ssDNA and dd-water weakens with increasing the base numbers. For the case of N=56, the interaction is too weak to form the transition channels for PL emission and, thus, to induce the Peak 1.

Akin to C35, the Peak 2 can be seen for $\lambda_{em}$=420 nm where the Peak 3 is absent, and both the Peak 2 and Peak 3 can been observed for $\lambda_{em}$=450 nm. It should be noted from our experimental measurements that the PLE spectra for G-based ssDNA are more complicated and richer in terms of physics and chemistry. For simplicity of the presentation and discussion we do not attempt to deal with the PLE spectrum for G-based samples in details in this article. The results shown in Fig. 4(a-c) indicate that the interaction of the double hydrogen bonds between C-base in ssDNA and dd-water plays an important role in affecting the features of PLE spectrum in relatively short $\lambda_{ex}$ regime. Such an effect has been applied[26] for the understanding of the light emission mechanism and of the characteristics in a strong double hydrogen bond formed after two ground state Pyrene molecules recombined with $F^-$ ions.

Furthermore, with the results shown in Fig. 1, we can also examine the dependence of the amplitude of the PL peak ($I_p$) upon the excitation wavelength $\lambda_{ex}$. In doing so, we apply the Gaussian fitting to the measured PL spectra in order to get more accurately the values of $I_p$. In Fig. 4(d), we plot $I_p$ as a function of $\lambda_{ex}$ for C28, A28, G28 and T28 samples. It is interesting to point out that one can clearly distinguish different samples by their peak amplitudes in the range of $\lambda_{ex}$=330~430 nm, from where we find that $I_G$> $I_A$> $I_T$> $I_C$. Such a finding is valid not only for the case of base number $N$=28 but also for the case of $N$=35 and 56 (not presented herewith).

On the basis of the results obtained from this study we find, from a viewpoint of physics, that the photo-induced light emission from ssDNA is akin to that from, e.g., a direct band-gap semiconductor with radiative impurity states[33-35]. The LUMO and

HOMO states in ssDNA serve as the conduction and valence bands in a semiconductor, where the electronic energy band structure and the corresponding density-of-states are determined by the nucleic acid structures as shown in insets in Fig. 1. Different bases of the ssDNA structures correspond to different electronic band structures. The PL peaks observed in region I in Fig. 1 and Fig. 2 are similar to those induced by excitonic transitions between the conduction and valence bands in a semiconductor, where the PL peak position depends only on the band-gap. Furthermore, the H-, O-, $CH_3$-, $NH_2$-, etc., bonds along with the water molecule bonds attached to the basic structure of A, T, C and G base can behave like the impurity states in a semiconductor. These functional groups are fluorophores for PL emission in long wavelength regime. The PL peaks in relatively long excitation wavelengths in Fig. 1 and the PLE peaks in Fig. 3 are similar to photo-induced light emission from radiative impurity sates in a doped semiconductor. The photo-induced light generation from impurity states in a semiconductor depends normally on the excitation wavelength[33-35].

The results obtained from this study indicate that for A-, T-, C- and G-based ssDNA, due to different base structures and functional groups attached to the base, the features of the PL emission look markedly different. Through examining the dependence of the PL and PLE peaks along with the amplitude of the PL peaks upon the excitation wavelength, we are able to identify optically the ssDNA with different bases and the same base but with different base numbers. Hence, one can achieve a non-invasive and label free characterization of the ssDNA samples by the standard PL measurement.

## Conclusions

In this work, we have studied the features of the photoluminescence (PL) from ssDNA with different bases A, T, C and G and base numbers 28, 35 and 56. The dependence of the PL emission from these samples upon excitation wavelength has been examined. The main conclusions drawn from this study can be summarized as follows.

1) In relatively short excitation wavelength regime, the PL emission from ssDNA is induced mainly via excitonic mechanism, where the peak wavelength $\lambda_{em}$ does not depend on the excitation wavelength $\lambda_{ex}$. In this excitation wavelength regime, the amplitude of the PL peak differs for ssDNA with different bases and base numbers.
2) In relatively long excitation wavelength regime, the PL emission from ssDNA is induced mainly via mechanisms of the dimer and water luminescences, where $\lambda_{em}$ depend strongly on $\lambda_{ex}$. In this regime, the features of the PL emission rely sensitively on the base structures of ssDNA. For example, the $\lambda_{em}$ ~$\lambda_{em}$ relation for T and A samples is roughly the same, whereas for C and G samples it exhibits the different characteristic dependences.
3) At a fixed emission wavelength $\lambda_{em}$, the PL excitation (PLE) spectrum in ssDNA comes from the formation of the radiative channels induced by the coupling of the hydrogen bonds in ssDNA and dd-water and from the dimer and dd-water luminescent channels. Accordingly, three PLE peaks can be found respectively at $\lambda_{em}$=308 nm, 345 nm and 397 nm for T-, A-, C- and G-based ssDNA. However, such a feature depends on the base number for a given base in ssDNA.

4) The amplitude of the PL peaks depends characteristically on the base structure of the ssDNA. It has been found that $I_G > I_A > I_T > I_C$ when $\lambda_{ex}$=330~430 nm for T, A, C and G samples at a fixed base number.

5) The physical mechanism of the PL emission from ssDNA is akin to that from a direct band-gap semiconductor with radiative impurity levels. The LUMO and HOMO states in ssDNA serve as the conduction and valence bands and the chemical bonds along with the water molecule bonds attached to the basic structure of A, T, C and G base can behave like the impurity states in a semiconductor. Thus, the features of the PL from ssDNA with different base structures can be understood with the help of semiconductor physics.

The most important and significant conclusion from this study is that through examining the dependence of the PL and PLE peaks along with the amplitude of the PL peaks upon the excitation wavelength, one can identify optically the ssDNA with different bases and the same base but with different base numbers. Consequently, one can achieve a non-invasive and label free characterization of the ssDNA samples by using a simple, low-cost and standard optical technique such as the PL measurement. We hope the interesting and important findings from this work can be helpful in gaining an in-depth understanding of the ssDNA with different base structures.

## Methods

### Preparation of samples

In this work, the ssDNA samples are prepared by using solid-phase phosphoramidite triester method with an automatic synthesizer (Bioautomation-MerMade-192E

DNA/RNA). The sequence of each ssDNA sample contains a certain amount of nucleobases of only one kind of A, C, T, and G base. For a given kind of nucleobase, we prepared the samples with the base number 28, 35 and 56. Table 1 shows the sequences for A, T, C and G based ssDNA with a base number $N$=28 as examples. The samples used in this study are in dd-water as solvent and the ssDNA concentration for all these samples is unified as 5 μmol/L.

Table 1: The base sequences of the ssDNA samples.

| Sample No. | Base(number) | Sequence |
|---|---|---|
| A28 | Adenine(28) | 5'-AAAAAAAAAAAAAAAAAAAAAAAAAAAA-3' |
| G28 | Guanine(28) | 5'-GGGGGGGGGGGGGGGGGGGGGGGGGGGG-3' |
| C28 | Cytosine(28) | 5'-CCCCCCCCCCCCCCCCCCCCCCCCCCCC-3' |
| T28 | Thymine(28) | 5'-TTTTTTTTTTTTTTTTTTTTTTTTTTTT-3' |

**Experimental setup and measurements**

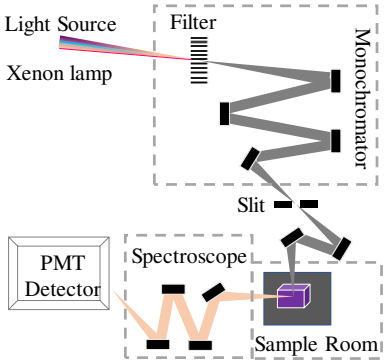


Fig. 5 Schematic diagram of the optical path for the PL measurement.

The PL and PLE spectra were measured by employing a multi-functional fluorescence system (HORIBA, USA), with the optical path shown in Fig. 5. A xenon lamp with radiation wavelength range from 240 nm to 850 nm is taken as the light source. The broadband light beam is monocolored by a monochromator (Gemini 180), which is used for tuning the excitation wavelength. Under the illumination of the excitation light, the PL emission from the sample can be detected by a grating spectrometer (iHR320)

together with a photomultiplier tube (PMT). In the measurement, the excitation light beam is applied at an angle of about 45° to the sample surface, and the detection is undertaken at about 60° to the sample surface. The accuracy of the spectral measurement can be up to 0.2 nm. The measurements in this study were carried out at room temperature.

**References**


1 Watson, J. D. & Crick, F. H. C. Molecular structure of nucleic acids - A structure for deoxyribose nucleic acid. *Am J Psychiat* 160, 623-624 (2003).

2 Seeman, N. C. Nucleic-Acid Junctions and Lattices. *J Theor Biol* 99, 237-247 (1982).

3 Zhang, H. Q., Li, F., Dever, B., Li, X. F. & Le, X. C. DNA-Mediated Homogeneous Binding Assays for Nucleic Acids and Proteins. *Chem Rev* 113, 2812-2841 (2013).

4 Angell, C., Xie, S. B., Zhang, L. F. & Chen, Y. DNA Nanotechnology for Precise Control over Drug Delivery and Gene Therapy. *Small* 12, 1117-1132 (2016).

5 Kumar, V. et al. DNA Nanotechnology for Cancer Therapy. *Theranostics* 6, 710-725 (2016).

6 Willner, I., Shlyahovsky, B., Zayats, M. & Willner, B. DNAzymes for sensing, nanobiotechnology and logic gate applications. *Chem Soc Rev* 37, 1153-1165 (2008).

7 Li, J. et al. Determination of calf thymus DNA using resonance light-scattering quenching method based on the terbium (Ш) ($Tb^{3+}$)/europium (Ш) ($Eu^{3+}$)–

quercetin system. *Journal of Luminescence* 129, 906-911 (2009).

8 Feng, S., Li, Z. P., Zhang, S. H. & Fang, Z. Recent advance of resonance light scattering technique for the determination of nucleic acids. *Spectrosc Spect Anal* 24, 1676-1680 (2004).

9 Qu, H., Hao, C., Nan, Z., Zhang, X. & Sun, R. Modulation of membrane properties by DNA in liposomes: A spectroscopic study. *Spectrochim Acta A Mol Biomol Spectrosc* 224, 117459 (2020).

10 Zhu, C. et al. Single-layer $MoS_2$-based nanoprobes for homogeneous detection of biomolecules. *J Am Chem Soc* 135, 5998-6001 (2013).

11 Kim, K. R. et al. Drug delivery by a self-assembled DNA tetrahedron for overcoming drug resistance in breast cancer cells. *Chem Commun* 49, 2010-2012 (2013).

12 Kim, K. R. et al. Sentinel lymph node imaging by a fluorescently labeled DNA tetrahedron. *Biomaterials* 34, 5226-5235 (2013).

13 Zhang, B. Z. & Wei, C. Y. Highly sensitive and selective detection of $Pb^{2+}$ using a turn-on fluorescent aptamer DNA silver nanoclusters sensor. *Talanta* 182, 125-130 (2018).

14 Enkin, N., Sharon, E., Golub, E. & Willner, I. Ag Nanocluster/DNA Hybrids: Functional Modules for the Detection of Nitroaromatic and RDX Explosives. *Nano Lett* 14, 4918-4922 (2014).

15 Petty, J. T., Zheng, J., Hud, N. V. & Dickson, R. M. DNA-templated Ag nanocluster formation. *J Am Chem Soc* 126, 5207-5212 (2004).

16 Maxwell, D. J., Taylor, J. R. & Nie, S. M. Self-assembled nanoparticle probes for recognition and detection of biomolecules. *J Am Chem Soc* 124, 9606-9612 (2002).

17 Zhang, L. B. et al. A new approach to light up DNA/Ag nanocluster-based beacons for bioanalysis. *Chem Sci* 4, 4004-4010 (2013).

18 Lin, X. D. et al. Multiple advanced logic gates made of DNA-Ag nanocluster and the application for intelligent detection of pathogenic bacterial genes. *Chem Sci* 9, 1774-1781 (2018).

19 Mcbride, L. J. & Caruthers, M. H. An investigation of several deoxynucleoside phosphoramidites. *Tetrahedron Letters* 24, 245–248 (1983).

20 Buck, H. M. The Risk of the Preparation of Artificial DNAs via an Interrupted Automated Solid-Phase Triester Method. *Nucleosides Nucleotides Nucleic Acids* 34, 400-415 (2015).

21 Li, C. et al. Photon-Induced Light Emission from Foamed Gold with Micro/Nanohollow Sphere Structures. *ACS Omega* 2, 5759-5765 (2017).

22 Christian, G. et al. N−H Stretching Excitations in Adenosine-Thymidine Base Pairs in Solution: Pair Geometries, Infrared Line Shapes, and Ultrafast Vibrational Dynamics. *J. Phys. Chem. A* 117, 594−606 (2013).

23 Fidder, H. et al. N-H stretching vibrations of guanosine-cytidine base pairs in solution: Ultrafast dynamics, couplings, and line shapes. *Journal of Physical Chemistry A Molecules Spectroscopy Kinetics Environment & General Theory* 117, 845−854 (2013).

24 Furse, K. E. & Corcelli, S. A. Molecular Dynamics Simulations of DNA Solvation Dynamics. *The Journal of Physical Chemistry Letters* 1, 1813-1820 (2010).

25 Zhang, L., Yang, Y., Kao, Y. T., Wang, L. & Zhong, D. Protein hydration dynamics and molecular mechanism of coupled water-protein fluctuations. *Journal of the American Chemical Society* 131, 10677-91 (2009).

26 Kim, S. K., Ju, H. B., Bartsch, R. A., Jin, Y. L. & Kim, J. S. A Fluoride-Selective PCT Chemosensor Based on Formation of a Static Pyrene Excimer. *Cheminform* 37, 4839-4842 (2006).

27 Murphy, K. R. A Note on Determining the Extent of the Water Raman Peak in Fluorescence Spectroscopy. *Applied Spectroscopy* 65, 233-236 (2011).

28 Harmon, A. D., Weisgraber, K. H. & Weiss, U. Preformed Azulene Pigments of Lactarius-Indigo (Schw) Fries (Russulaceae, Basidiomycetes). *Experientia* 36, 54-56 (1980).

29 Kang, H., Jung, B. & Kim, S. K. Mechanism for ultrafast internal conversion of adenine. *J Chem Phys* 118, 6717-6719 (2003).

30 Fuji, T., Ong, H. J. & Kobayashi, T. Real-time observation of vibrational coherence persisting after internal conversion and vibrational relaxation in cyanine dye molecules. *Chemical Physics Letters* 380, 135-140, (2003).

31 Schrader, T. et al. Vibrational relaxation following ultrafast internal conversion: comparing IR and Raman probing. *Chemical Physics Letters* 392, 358-364, (2004).

32 Roland, Langner, & Georg, Zundel. Ft-ir investigation of $OH\cdots N \rightleftharpoons O^{-}\cdots H^{+}N$ hydrogen bonds with large proton polarizability in phosphinic acid + N-base systems in the middle and far infrared region. *Journal of Physical Chemistry A* 102, 6635-6642 (1998).

33 Ertap, H., Bacıoğlu, A. & Karabulut, M. Photoluminescence properties of boron doped InSe single crystals. *Journal of Luminescence* 167, 227-232 (2015).

34 Ardekani, H., Younts, R., Yu, Y., Cao, L. & Gundogdu, K. Reversible Photoluminescence Tuning by Defect Passivation via Laser Irradiation on Aged Monolayer $MoS_2$. *ACS Appl Mater Interfaces* 11, 38240-38246 (2019).

35 Chiranjeevi Maddi. et al. Structural, Spectroscopic, and Excitonic Dynamic Characterization in Atomically Thin $Yb^{3+}$-Doped $MoS_2$, Fabricated by Femtosecond Pulsed Laser Deposition. *Advanced Optical Materials* 7, 1900753-1900762 (2019).

**Acknowledgements**

This work was supported by the National Natural Science Foundation of China (Grant Numbers: 11764045, U1832153, U1930116) and the Ten-thousand Talents Program of Yunnan Province (YNWR-QNBJ-2018-037).